Simultaneous Identification and Control for Hybrid Energy Storage System Using Model Predictive Control and Active Signal Injection

Ziyou Song, *Member, IEEE*, Hyeongjun Park, *Member, IEEE*, Fanny Pinto Delgado, *Student Member, IEEE*, Hao Wang, Zhaojian Li, *Member, IEEE*, Heath F. Hofmann, *Senior Member, IEEE*, Jing Sun, *Fellow, IEEE*, and Jun Hou, *Member, IEEE*

***Abstract*—A battery/supercapacitor hybrid energy storage system (HESS) is overactuated in the sense that there are two power sources providing a single power output. This feature of HESS is exploited in this article to simultaneously achieve accurate identification of the battery states/parameters and high system efficiency. By actively injecting current signals, the state of charge and state of health, together with other battery parameters, can be identified sequentially. Sufficient richness in the input (i.e., battery current) is necessary to ensure identification accuracy. Since signal richness for identification can be in conflict with efficient operation, a novel model predictive control (MPC) strategy is used to simultaneously consider both objectives to determine the optimal power distribution between supercapacitor and battery. The tradeoff between identification accuracy and system efficiency is investigated. Simulation results show that the proposed MPC can significantly improve identification accuracy at the expense of a slight decrease in system efficiency when compared to the baseline MPC, which does not consider the signal richness. Therefore, it is validated that the proposed MPC can effectively achieve simultaneous identification and efficient operation.**

***Index Terms*—Hybrid energy storage system (HESS), lithium-ion battery, model predictive control (MPC), overactuated nature, state of charge (SoC)/state of health (SoH) identification.**

Manuscript received February 4, 2019; revised August 12, 2019; accepted October 27, 2019. Date of publication November 15, 2019; date of current version July 14, 2020. This work was supported by U.S. Office of Naval Research under Grant N00014-16-1-3108 and Grant N00014-18-2330. *(Corresponding author: Jun Hou.)*

Z. Song, H. Wang, and J. Sun are with the Department of Naval Architecture and Marine Engineering, University of Michigan, Ann Arbor, MI 48109 USA (e-mail: ziyou.songthu@gmail.com; autowang@umich.edu; jingsun@umich.edu).

H. Park is with the Department of Mechanical and Aerospace Engineering, New Mexico State University, Las Cruces, NM 88003 USA (e-mail: hjpark@nmsu.edu).

F. P. Delgado, H. F. Hofmann, and J. Hou are with the Department of Electrical Engineering and Computer Science, University of Michigan, Ann Arbor, MI 48109 USA (e-mail: fapd@umich.edu; hofmann@umich.edu; junhou@umich.edu).

Z. Li is with the Department of Mechanical Engineering, Michigan State University, East Lansing, MI 48824 USA (e-mail: lizhaoj1@egr.msu.edu).

Color versions of one or more of the figures in this article are available online at http://ieeexplore.ieee.org.

Digital Object Identifier 10.1109/TIE.2019.2952825

NOMENCLATURE

a	OCV–SoC slope (V/%).
b	Constant of linearized OCV–SoC curve (V).
C_{SC}	SC capacitance (F).
C_t	Capacitance of *RC* pair (F).
i_b	Battery current (A).
$i_{b,\max}$	Maximum battery current (A).
$i_{b,\min}$	Minimum battery current (A).
I_{ex}	Amplitude of the injected current (A).
i_{ex}	Injected current (A).
$I_{ex,\max}$	Maximum injected current (A).
$I_{ex,\min}$	Minimum injected current (A).
i_{SC}	Supercapacitor current (A).
$i_{\mathrm{SC},\max}$	Maximum supercapacitor current (A).
$i_{\mathrm{SC},\min}$	Minimum supercapacitor current (A).
K_0–K_4	Coefficients of OCV–SoC curve.
N	Prediction horizon.
P_b	Battery power (kW).
P_d	Power demand (kW).
P_{SC}	Supercapacitor power (kW).
Q_b	Battery capacity (Ah).
R_s	Ohmic resistance of battery (Ω).
$\widehat{R_s}$	Estimated ohmic resistance (Ω).
R_{SC}	Supercapacitor resistance (Ω).
R_t	Resistance of *RC* pair (Ω).
s	Complex Laplace variable.
SoC_b	Battery SoC (%).
$\mathrm{SoC}_{b,\max}$	Maximum battery SoC (%).
$\mathrm{SoC}_{b,\min}$	Minimum battery SoC (%).
$\mathrm{SoC}_{\mathrm{SC}}$	Supercapacitor SoC (%).
$\mathrm{SoC}_{\mathrm{SC},\max}$	Maximum supercapacitor SoC (%).
$\mathrm{SoC}_{\mathrm{SC},\min}$	Minimum supercapacitor SoC (%).
t	Time (s).
t_0	Start time (s).
T_s	Sampling time (s).
v_b	Battery terminal voltage (V).
v_C	Voltage over the *RC* pair (V).
v_{OC}	Open-circuit voltage of battery (V).
v_{SC}	Open-circuit voltage of supercapacitor (V).
$v_{\mathrm{SC},\max}$	Maximum voltage of supercapacitor (V).

v_t	Supercapacitor terminal voltage (V).
z	Battery SoC (%).
z_0	Battery initial SoC (%).
η	Coulombic efficiency of battery (%).
λ_1, λ_2	Weighting parameters.
τ	Time constant of the *RC* pair (s).

Acronyms

CR	Cramer–Rao.
ECM	Equivalent circuit model.
EKF	Extended Kalman filter
HESS	Hybrid energy storage system
MPC	Model predictive control
OCV	Open-circuit voltage
RMS	Root-mean-square
SC	Supercapacitor
SIC	Simultaneous identification and control
SoC	State of Charge
SoH	State of Health

I. Introduction

PARAMETER identification and system optimization are often conflicting objectives, with identification requiring persistently exciting inputs for parameter convergence [1], while system optimization objectives generally minimize a predefined cost function that does not generate persistently exciting inputs. While these conflicting objectives cannot be simultaneously achieved for most systems overactuated systems in which the number of inputs is greater than the number of outputs [2] can be exploited for SIC. Overactuated systems provide an opportunity to introduce excitation for parameter identification in such a way that it does not perturb regulated outputs [1].

Similar work, which trades off parameter identification and output regulation objectives can be found in the literature. For example, Reed *et al.* exploited the overactuation of permanent magnet synchronous machines (PMSMs) to achieve parameter identification and torque regulation objectives simultaneously [3]. Hasanzadeh *et al.* [4] also focused on the PMSM and estimated the rotor resistance by injecting a relatively low-frequency carrier signal, and then the overactuation feature was utilized to minimize the torque ripple by the carrier signal. Chen and Wang [5] used the additional degrees of freedom in an electric vehicle with independent motors to provide additional excitation for accurate tire-road friction coefficient estimation. Similarly, Leve and Jah exploited the "null motion" of an overactuated spacecraft to add excitation for parameter identification without disturbing the control objective [6].

The battery/SC HESS has been widely used in transportation [7] and grid [8] applications, given that the adoption of SC is an effective solution to prolong battery lifetime [9]. HESS is an overactuated system since there are two inputs, i.e., the output power of SC and battery, and a single output, i.e., the demand power required by the load. Therefore, HESS offers an additional degree of freedom which can be potentially utilized to improve parameter identification performance [10]. We point out that the overactuated nature of HESS is worthy of investigation because accurate identification of parameters/states, such as battery SoC and SoH, plays an important role in ensuring reliable and efficient operation [11]. However, most existing studies of HESS focus on topology optimization [12], component sizing [13], and design of the energy management strategy [14]. The overactuated nature of HESS has been neglected.

The SC can be represented by a simple model and, therefore, simply characterized [15]. However, the concurrent identification of battery SoC/SoH together with its model parameters, which are significantly influenced by battery degradation and operating conditions [16], is still challenging considering measurement noise and model inaccuracy [17]. It has been proven that identification accuracy can be impaired when data without rich information is used [18], even though most existing studies use data indiscriminately [19]. Recently, more attention has been paid to the impact of data on the identification performance of battery parameters. Lin and Stefanopoulou [20] and Klintberg *et al.* [21] used the CR bound to quantify the influence of data on identification accuracy. Rothenberger *et al.* [22] optimized the battery current profile to maximize the Fisher information matrix and, therefore, improve identification performance, [23]. The connection between excitation input and SoC estimation error considering sensor bias and variance has also been investigated [24]. It has been shown that the identification performance of a sequential algorithm, which identifies battery parameters and states sequentially by actively injecting current signals, can be significantly improved when compared to the case where all battery parameters and states are estimated concurrently [25].

Even though the aforementioned literatures have pointed out that the current profile significantly influences the identification accuracy of battery parameters/states and it is worthwhile actively injecting optimal signals to battery, none of them have implemented such an algorithm in practical applications. This article extends the framework of the original SIC by considering system efficiency in addition to identification and control objectives.

This is the first article, this article is the first to consider optimization objectives and identification accuracy simultaneously, and realizes active signal injection into the battery to increase the identification accuracy in an overactuated system when the system can normally work in practical conditions.

To actively inject the excitation current, the overactuated feature of HESS, which has been widely used in electric vehicles [12] and all-electric ships [26], is exploited using MPC [27], which has been explored as a framework for SIC [28]–[30]. MPC is used in this article to simultaneously consider the signal richness for identification and HESS efficiency by optimally distributing power between SC and battery. Simulation results show that the proposed MPC can significantly improve identification accuracy at the expense of a slight reduction in system efficiency when compared to a baseline MPC which does not consider signal richness. In addition, the tradeoff between identification accuracy and HESS efficiency is investigated.

This is the first article utilizing the overactuation feature to actively inject signals into a battery in use, thereby significantly improving the estimation accuracy of battery states/parameters. This improvement is crucial to the safe, efficient, and reliable

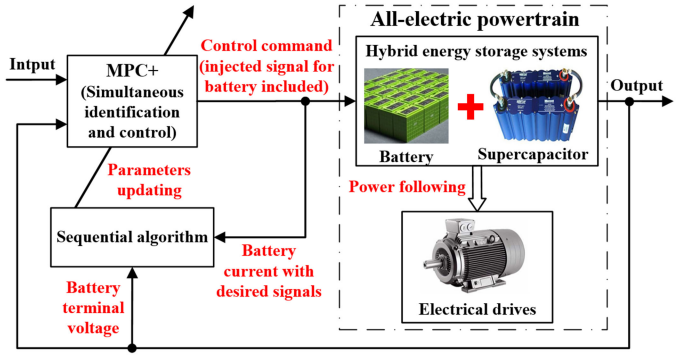

Fig. 1. Schematic of the proposed SIC for HESS.

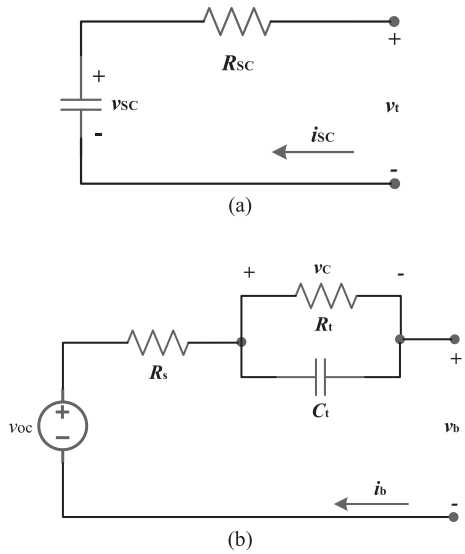

Fig. 2. Equivalent circuit model of HESS. (a) SC model. (b) Battery model.

operation of Lithium-ion batteries. Specifically, the proposed algorithm can avoid the inherent uncertainties involved in the estimation process by compromising with slightly more energy consumption.

The rest of this article is organized as follows. In Section II, simultaneous identification and optimization is introduced and the HESS model is described. In Section III, formulations of the baseline MPC and proposed MPC are presented. Simulation results are provided and analyzed in Section IV. Section V concludes this article.

II. Hybrid Energy Storage System

A. Simultaneous Identification and Control Objective

The HESS under investigation has two power sources (i.e., SC and battery) and provides output power to a single load, as shown in Fig. 1. Thus, the power output of each energy storage can vary while keeping the total output power constant. The overactuated nature of HESS provides a perfect opportunity to address the SIC problem, which ensures that a sufficient condition for accurate parameter identification (i.e., persistently exciting inputs) is maintained in addition to achieving a control objective (e.g., output regulation) [1]. A persistently exciting input is especially important for the battery since it is difficult to simultaneously identify all battery parameters and states [25].

This article considers system efficiency in addition to identification and control objectives. Specifically, an excitation current of a desired frequency is injected to achieve battery parameter/state identification. Then, the signal richness, which has been proven to be linearly proportional to the amplitude of the injected current [17], and the system efficiency are optimized through a weighted-sum method to convert the multi-objective optimization problem (i.e., system efficiency and identification accuracy) into a single-objective optimization problem, while the output power of the HESS is accurately controlled to follow the power demand. While identification and control can be simultaneously achieved without compromise by exploiting the overactuated feature of HESS, identification and optimization are still conflicting objectives for overactuated systems since in general the optimal solutions for maximizing system efficiency do not include an input with sufficient richness for identification. Therefore, the goal of this article is to achieve the best tradeoff between these competing objectives. Note that the proposed SIC is dealing with a time-varying system as the battery parameter is continuously estimated by the sequential algorithm and then fed back to the proposed MPC, which attempts to simultaneously minimize the energy loss and maximize the signal richness.

B. Equivalent Circuit Models for Battery and Supercapacitor

In the proposed SIC framework, the cost function accounts for the power losses of both SC and battery, which are calculated based on ECMs.

The SC ECM can be simplified to an *RC* circuit, as shown in Fig. 2(a) [10]. The SC OCV, terminal voltage, resistance, and current are denoted as v_{SC}, v_t, R_{SC}, and i_{SC} (positive for discharging and negative for charging), respectively. The SoC of SC is linearly proportional to its OCV and therefore can be easily estimated [12]

$$\mathrm{SOC}_{\mathrm{SC}}(t) = \mathrm{SOC}_{\mathrm{SC}}(0) - \int_0^t \frac{i_{\mathrm{SC}}(t)}{C_{\mathrm{SC}} v_{\mathrm{SC,\,max}}} dt \tag{1}$$

where t is the time instant, C_{SC} is the SC capacitance, and $v_{\mathrm{SC,max}}$ is the SC maximum voltage. In contrast, the ECM for representing the battery dynamics is more complicated. Among all existing models, the first-order ECM, as shown in Fig. 2(b), is widely used in practical applications due to its sufficient accuracy and low computational cost [31]. Therefore, it is also adopted in this paper for battery state/parameter identification.

As shown in Fig. 2(b), the battery terminal voltage is defined as v_b and the battery current is defined as i_b. The first-order ECM dynamics can be derived as follows:

$$\begin{cases} \dot{v}_C = -\frac{1}{\tau} v_C + \frac{R_t}{\tau} i_b, \\ v_b = v_{\mathrm{OC}} - R_s i_b - v_C \end{cases} \tag{2}$$

where v_C is the voltage over the *RC* pair and $\tau = R_t C_t$ is the time constant. The OCV–SoC curve can be expressed as follows [32]:

$$v_{\mathrm{OC}}(z) = K_0 - \frac{K_1}{z} - K_2 z + K_3 \ln(z) + K_4 \ln(1-z) \quad (3)$$

where K_0–K_4 are the model coefficients and z is the normalized SoC, and the SoC dynamic is given by the following [33]:

$$z = z_0 - \int_{t_0}^{t} \frac{\eta}{Q_b} i_b(t) dt \quad (4)$$

where z_0 is the initial SoC, η is the charging/discharging efficiency, t_0 is the start time, and Q_b is the battery capacity. For the combined state and parameter estimation problem studied in this article, we assume that the values of R_s, R_t, and τ are constant in the estimation process, since they vary much more slowly than the battery SoC [34].

C. Brief Review of Sequential Algorithm

The identification of battery states (e.g., SoC and SoH) and parameters is an important and difficult task in practical applications, but identification accuracy is limited when identifying all parameters and states simultaneously due to noise and unmodeled dynamics. The sequential algorithm is proposed to solve this problem. Identifying battery parameters/states sequentially by incorporating a high-pass filter and actively injecting current has been proven to significantly improve identification accuracy [25]. The sequential algorithm was designed based on battery dynamic analysis in the frequency domain [25]. To simplify the analysis, (3) is linearized given that the slope of the OCV–SoC curve is constant for most battery chemistries within the normal operating range [35]

$$v_{\mathrm{OC}}(t) = a\left(z_0 - \int_{t_0}^{t} \frac{\eta i_b(v)}{Q_b} \mathrm{d}v\right) + b \quad (5)$$

where a and b are the coefficients of the linearized OCV–SoC function. Based on (2)–(5), the battery dynamics in the frequency domain can be derived using the Laplace transform

$$v_b(s) = \left[\frac{a z_0}{s} + \frac{b}{s}\right] - \left[\frac{a}{s}\frac{\eta}{Q_b} i_b(s)\right] - [R_s i_b(s)] - \left[\frac{R_t}{1+\tau s} i_b(s)\right] \quad (6)$$

where s is the complex Laplace variable. As shown in (6), the battery terminal voltage includes four components, which are dominated by the initial SoC, SoC variation, ohmic resistance, and *RC* pair, respectively. These four components have significantly different dynamic characteristics, and can be decomposed by incorporating high-pass filters and actively injecting current. Specifically, by using the high-pass filter, the first term associated with the initial SoC can be removed because it is constant. As for the filtered system, when the current frequency is high, the battery voltage is dominated by the ohmic resistance drop. At medium frequency the term associated with the SoC variation can be neglected and the battery voltage is dominated by the ohmic resistance and *RC* pair. Therefore, the sequential algorithm can be summarized in the following three steps [25].

Step #1: By incorporating a high-pass filter and injecting high-frequency current, the ohmic resistance is identified using the EKF.

Step #2: The estimated ohmic resistance is used. By incorporating a high-pass filter and injecting medium-frequency current, R_t and τ are identified using the EKF.

Step #3: The estimated R_s, R_t, and τ are adopted. Hence, the SoC and SoH can be simultaneously estimated based on the unfiltered system. A dual EKF, which can identify the states and parameters concurrently, is employed.

III. Simultaneous Identification and Control Using Model Predictive Controller

MPC is used in this article to solve the SIC problem, deal with constraints, and regulate the HESS output power. The baseline MPC, which does not consider current injection, is first introduced. The baseline MPC is denoted as MPC–, and the states and inputs of MPC– are defined as follows:

$$x(k) = \begin{bmatrix} \mathrm{SoC}_b(k) \\ \mathrm{SoC}_{\mathrm{SC}}(k) \end{bmatrix}, \quad u(k) = \begin{bmatrix} i_b \\ i_{\mathrm{SC}}(k) \end{bmatrix}. \quad (7)$$

Note that the control horizon of i_b is chosen to be 1 for a fair comparison with the proposed MPC, which will be described later. The optimization problem of MPC– is formulated as follows:

$$J_{\mathrm{MPC-}}(x(k), u(k)) = \sum_{k=0}^{N} \left[R_s i_b^2 + R_{\mathrm{SC}} i_{\mathrm{SC}}^2(k)\right] + \lambda_1 [v_{\mathrm{SC}}(k) - 0.9 v_{\mathrm{SC,max}}]^2 \quad (8)$$

subject to the constraints

$$\mathrm{SoC}_{b,\min} \le \mathrm{SoC}_b \le \mathrm{SoC}_{b,\max},$$

$$\mathrm{SoC}_{\mathrm{SC},\min} \le \mathrm{SoC}_{\mathrm{SC}} \le \mathrm{SoC}_{\mathrm{SC},\max},$$

$$i_{b,\min} \le i_b \le i_{b,\max},$$

$$i_{\mathrm{SC},\min} \le i_{\mathrm{SC}} \le i_{\mathrm{SC},\max},$$

$$\sum_{k=0}^{N} |P_d - P_b(k) - P_{\mathrm{SC}}(k)| \le \varepsilon,$$

$$x(k+1) = \begin{bmatrix} 1 & 0 \\ 0 & 1 \end{bmatrix} x(k) - \begin{bmatrix} \frac{T_s}{3600 Q_b} & 0 \\ 0 & \frac{T_s}{v_{\mathrm{SC,max}} C_{\mathrm{SC}}} \end{bmatrix} u(k)$$

where $J_{\mathrm{MPC-}}$ is the cost function of MPC–, N is the prediction horizon, λ_1 is the weighting parameter that allows us to put a different emphasis on each objective, k is the time instant, v_{SC} is the SC voltage, $v_{\mathrm{SC,max}}$ is the maximum voltage of SC, $\mathrm{SoC}_{b,\min}$ ($\mathrm{SoC}_{b,\max}$) and $\mathrm{SoC}_{\mathrm{SC},\min}$ ($\mathrm{SoC}_{\mathrm{SC},\max}$) are the lower (upper) boundaries of the SoC of the battery and SC, respectively, $i_{b,\min}$ ($i_{b,\max}$), and $i_{\mathrm{SC},\min}$ ($i_{\mathrm{SC},\max}$) are the lower (upper) boundaries of the current of the battery and SC, respectively, P_b and P_{SC} are the battery and SC power, P_d is the power demand, ε is a small

allowable error for the output power regulation, Q_b is the battery capacity, $C_{\rm SC}$ is the SC capacitance, and T_s is the sampling time (e.g., 1s for MPC–). In the cost function of baseline MPC, HESS power loss and SC usage are concurrently considered.

The reference value of SC SoC is set to 0.9 to give the SC some storage capacity to absorb regenerative braking energy [14]. The cost term associated with the SC SoC reference aims to address the limitation of a short predictive horizon and use the SC more effectively [26]. Note that P_d is assumed to be constant in the prediction horizon, meaning that the power demand prediction is not considered in this study. The SC SOC is strictly controlled above 50% because the efficiency of power conversion becomes poor when the SC voltage is low. In addition, the battery voltage is assumed to be constant to simplify the calculation because the variation of battery voltage is generally small in its normal operating range [14]. Output regulation is realized by a nonlinear constraint. In addition, the *RC* pair is neglected in the calculation of battery power loss, since the time constant of the Lithium-ion battery in this study is more than 15 s, while the sampling period of MPC is less than 1 s. Therefore, the battery current mainly flows through the capacitor in the *RC* pair and the dynamics associated with the *RC* pair can be neglected.

A sinusoidal battery current, which is frequently used for parameter estimation, is injected for the sequential algorithm to identify battery parameters/states

$$i_{ex}(t) = I_{ex}\cos(2\pi f t) \tag{9}$$

where i_{ex} is the injected current, I_{ex} is the current amplitude, and f is the current frequency. It has been proven that the identification accuracy is proportional to the amplitude of excitation current [10]. Hence, the proposed MPC, denoted as MPC+, not only ensures that the excitation current of desired frequencies are injected but also takes the signal magnitude (i.e., I_{ex}) into consideration. The state of MPC+ is the same as that of MPC–, and the amplitude of excitation current is added to the inputs of MPC+

$$u(k) = \begin{bmatrix} i_b \\ i_{\rm SC}(k) \\ I_{ex} \end{bmatrix}. \tag{10}$$

The control horizons of i_b and I_{ex} are both chosen as 1 s to ensure the successful injection of excitation current. Otherwise, the injected signal will be compensated by i_b and disappear in the battery current profile, since minimizing the system power loss and increasing the signal richness for identification are inherently conflicting objectives. Note that i_b is also set to be constant in the prediction horizon in the cost function of the baseline MPC, as shown in (8), in order to have a fair comparison. The optimization problem of MPC+ is defined as follows:

$$\begin{aligned} J_{\rm MPC+}(x(k), u(k)) = &\sum_{k=0}^{N} \Big[\hat{R}_s(i_b + I_{ex}\cos(2\pi f T_s k))^2 \\ &+ R_{\rm SC} i_{\rm SC}^2(k)\Big] \\ &+ \lambda_1[v_{\rm SC}(k) - 0.9 v_{\rm SC,max}]^2 + \lambda_2 \frac{1}{I_{ex}^2} \end{aligned} \tag{11}$$

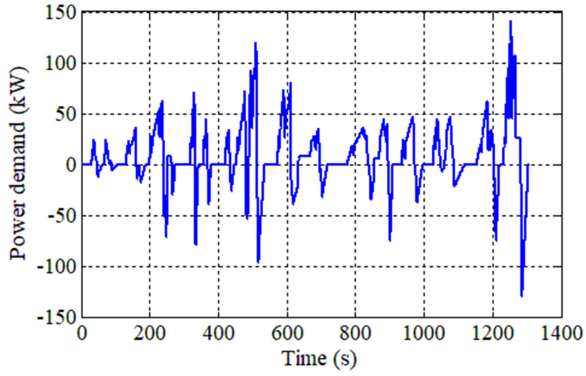

Fig. 3. Power demand profile related to a typical bus driving cycle.

subject to the constraints

$$\begin{aligned} &{\rm SoC}_{b,\min} \le {\rm SoC}_b \le {\rm SoC}_{b,\max}, \\ &{\rm SoC}_{\rm SC,min} \le {\rm SoC}_{\rm SC} \le {\rm SoC}_{\rm SC,max}, \\ &I_{b,\min} \le i_b \le I_{b,\max}, \\ &I_{\rm SC,min} \le i_{\rm SC} \le I_{\rm SC,max}, \\ &I_{ex,\min} \le I_{ex} \le I_{ex,\max}, \\ &\sum_{k=0}^{N} |P_d - P_b(k) - P_{\rm SC}(k)| \le \varepsilon, \\ &x(k+1) = \begin{bmatrix} 1 & 0 \\ 0 & 1 \end{bmatrix} x(k) \\ &\qquad - \begin{bmatrix} \frac{T_s}{3600 Q_b} & 0 & \frac{\cos(2\pi f T_s k) T_s}{3600 Q_b} \\ 0 & \frac{T_s}{v_{\rm SC,max} C_{\rm SC}} & 0 \end{bmatrix} u(k) \end{aligned}$$

where $J_{\rm MPC+}$ is the cost function of MPC+, λ_2 is the weighting parameter for the signal amplitude, $\widehat{R_s}$ is the estimated ohmic resistance, and $I_{ex,\min}$ ($I_{ex,\max}$) is the lower (upper) boundary of the excitation current amplitude. The sampling time of MPC+ depends on the frequency of the injected signal, and T_s is set to 0.2 and 1 s for injecting current signals of 0.5 and 0.05 Hz, respectively.

Remark: Note that the estimated resistance is also used in the optimization. When compared to the traditional estimation and optimization formulations [27], the advantage of this novel SIC framework is that the persistently exciting inputs for the parameter estimation are guaranteed by the proposed MPC. Therefore, the estimated parameter will converge to its actual value, and in turn, it can be used in the optimization to improve system performance.

IV. Simulation Results

A. System Optimization

A power demand profile corresponding to a typical bus driving cycle shown in Fig. 3 is adopted, given that HESS has been widely used in transportation applications [12]. Therefore, the sizes of the battery and SC packs are scaled to those of an

TABLE I
SPECIFICATION FOR THE MPC FORMULATION

Parameter	Value
Prediction horizon N	10
Resistance of the battery pack R_s (mΩ)	64
Resistance of the SC pack R_{SC} (mΩ)	43
Battery pack capacity Q_b (Ah)	300
SC pack capacitance C_{SC} (F)	63
Battery pack voltage (V)	384
Maximum voltage of SC pack $v_{SC,max}$ (V)	625
Battery current boundaries $I_{b,min}/I_{b,max}$ (A)	-200/200
SC current boundaries $I_{SC,min}/I_{SC,max}$ (A)	-240/240
Battery SoC boundaries $SoC_{b,min}/SoC_{b,max}$ (%)	20/90
SC SoC boundaries $SoC_{SC,min}/SoC_{SC,max}$ (%)	50/99
Boundaries of excitation current amplitude $I_{ex,min}/I_{ex,max}$ (A)	5/10
Tolerance of the output power regulation ε (kW)	0.1

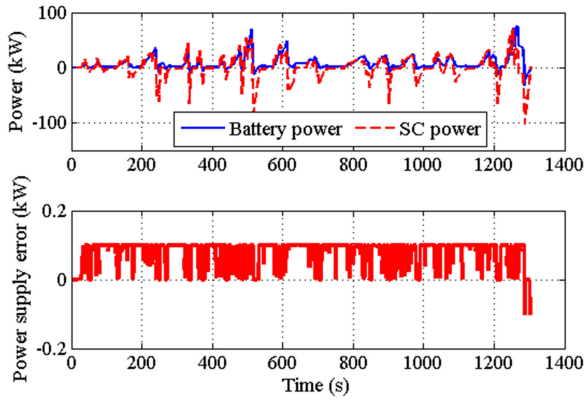

Fig. 4. Power split results of baseline MPC– without current injection.

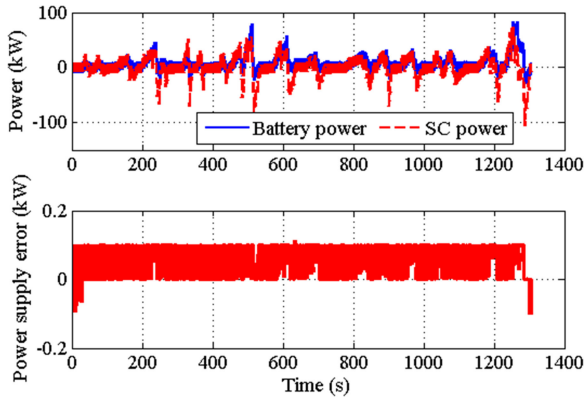

Fig. 5. Power split results of MPC+ with the injected current frequency of 0.5 Hz.

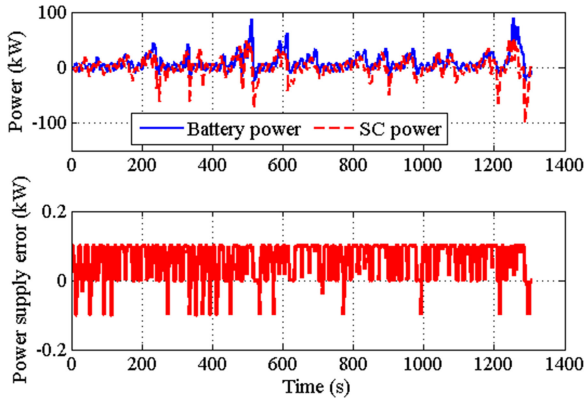

Fig. 6. Power split results of MPC+ with the injected current frequency of 0.05 Hz.

electric bus [14]. The specifications of HESS and MPC–/MPC+ are listed in Table I. The weighting parameters λ_1 and λ_2 are determined through trial-and-error, and λ_1 is set to 4 for the MPC– to achieve optimal performance (i.e., minimum energy loss). The "fmincon" MATLAB function is used to solve all MPC problems in this article [36]. As shown in Fig. 4, MPC– effectively distributes the power between the SC and battery, while the demand power is accurately followed by the HESS. The SoC of SC fluctuates in a wide range to supply/absorb high power demands, meaning that the SC is effectively used. The battery only supplies low and "constant" power, therefore its life span can be significantly prolonged. The energy consumption of HESS during the entire driving cycle is 9899.76 kJ.

For the proposed MPC+, a sinusoidal current of 0.5 Hz is actively injected first to identify the ohmic resistance. The sampling time is set to 0.2 s considering the frequency of the injected current. Based on the simulation results, the weighting parameters λ_1 and λ_2 in the cost function of MPC+ are set to 20 and 1000, respectively. Note that λ_1 is increased in the MPC+ based on trial-and-error when compared to the one in MPC– (i.e., 4). In both MPC– and MPC+, λ_1 and λ_2 are tuned manually to achieve optimal performance in order to enable a fair comparison between different algorithms. Under the proposed MPC+, the power demand is well followed, indicating a satisfactory output regulation performance as shown in Fig. 5. In addition, the desired excitation is successfully injected in the battery current profile, and the fluctuations in the SC current profile compensate the negative influence of the injected current on the output regulation. Therefore, the SIC is well addressed by the proposed MPC+. As for the SIC, the simulation result shows that the energy consumption of HESS during the entire cycle is 9940.83 kJ, revealing that MPC+ has a compromise of 0.4% increase when compared to MPC–. The identification results and the tradeoff between identification and loss minimization, which verify the proposed MPC+ can effectively perform SIC, will be presented in the sequel.

Simulation results which involve actively injecting a current of 0.05 Hz are shown in Fig. 6. The sampling time is increased to 1 s, and the weighting parameters λ_1 and λ_2 in the cost function of MPC+ are set to 4 and 200, respectively. The energy consumption of HESS is 9936.85 kJ, which has a 0.37% increase when compared to the MPC–.

To better present the excitation current injection, the characteristics of the current profiles corresponding to different cases are analyzed in the frequency domain using the fast Fourier transform, as shown in Fig. 7. This shows that the desired excitation current, which is necessary for the sequential algorithm, therefore can be successfully injected by the proposed MPC+. It is validated that the proposed MPC+ can ensure that persistently

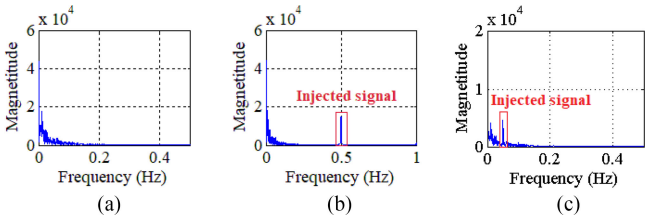

Fig. 7. Current profile in the frequency domain. (a) No excitation. (b) 0.5 Hz excitation. (c) 0.05 Hz excitation.

TABLE II
SPECIFICATIONS FOR THE 18650 BATTERY CELL

Parameter	Value
Nominal Voltage (V)	3.63
Cell Capacity (Ah)	2.44
Ohmic Resistance R_s (mΩ)	100
Diffusion Resistance R_t (mΩ)	33
Time Constant τ (s)	17
Discharge/Charge Efficiency η (%)	98
OCV-SoC slope a (mV/100%)	~8.845

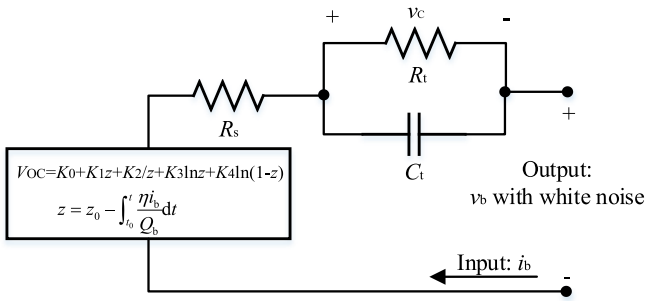

Fig. 8. Simulation model of the first-order circuit.

exciting signals with the desired frequency content always exist. In comparison, for the baseline MPC, the persistently exciting condition cannot be guaranteed. For example, when the power demand is 0, both the battery current and the supercapacitor current are 0, therefore battery parameter/state estimation cannot be conducted.

B. Battery Parameter/State Identification

Parameter/state identification of a battery was conducted in simulation. A Samsung 18650 lithium-ion, introduced in [17], is adopted in this article, and all battery current profiles are scaled (the scale ratio is 0.08) to fit the single cell, whose specifications are listed in Table II. As shown in Fig. 8, the simulation is conducted based on the first-order ECM, whose voltage is governed by the same dynamics as the adopted battery cell [see (2) and (3)]. The coefficients K_0–K_4 of the OCV–SoC for the adopted cell are 2.6031, 0.0674, −1.527, 0.6265, and −0.0297, respectively.

For a fair comparison, the initial guesses of the identified parameters and states are the same for MPC+ and MPC–, which are $[R_s(0)\ R_t(0)\ \tau(0)\ 1/Q_b(0)\ \mathrm{SoC}_b(0)]^{\mathrm{T}} = [0.02\Omega\ 0.01\Omega\ 10\,\mathrm{s}\ 1/2\mathrm{Ah}^{-1}\ 50\%]^{\mathrm{T}}$. The sequential algorithm is

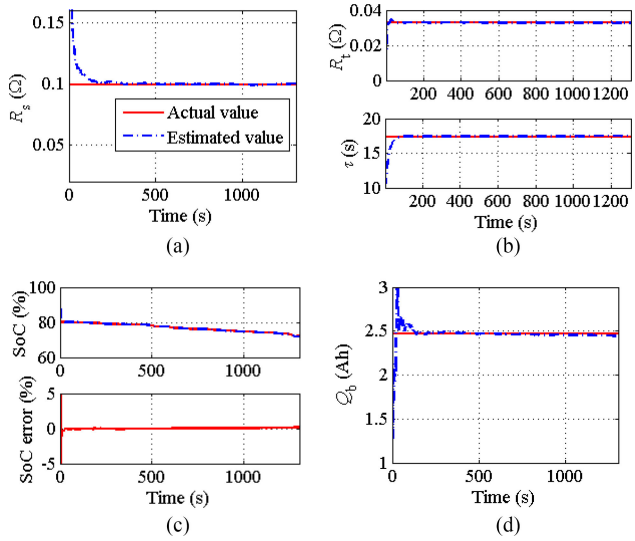

Fig. 9. Parameter identification result of MPC+. (a) R_s (Step #1). (b) R_t and τ (Step #2). (c) SoC (Step #3). (d) Q_b (Step #3).

used to identify the battery states/parameters based on the results of MPC+. In Step #1, a first-order butterworth high-pass filter with 3 dB bandwidth of 0.1 Hz is chosen based on the current characteristics shown in Fig. 7(b). The ohmic resistance R_s is identified using the EKF. As shown in Fig. 9(a), the identified value can accurately track the actual value. In Step #2, a first-order butterworth high-pass filter is designed with a 3 dB bandwidth of 0.008 Hz based on the result shown in Fig. 7(c). The identified R_s obtained from Step #1 is used, therefore R_t and τ can be accurately identified by the EKF, as shown in Fig. 9(b).

In Step #3, based upon the above identified parameters, a combined SoC and SoH identification is conducted using the dual EKF, which can estimate the parameters and states simultaneously. The detailed information about the sequential algorithm can be found in [25]. This previous study showed that the identification of SoC and SOH does not influence each other, and both prefer high OCV–SoC rate and current amplitude [17]. In addition, the identification of SoC is not influenced by the current frequency, while the identification of SoH prefers low current frequencies [25]. As a result, no excitation current needs to be injected and the battery current profile derived from MPC– can be used, which means that we switch from MPC+ to MPC– in Step #3. As shown in Fig. 9(c), the identified SoC follows the actual value accurately and the identification error is below 0.5%. In addition, the identified capacity converges to the actual value after 150 s, as shown in Fig. 9(d).

Hence, a satisfactory SoC and SoH identification performance is achieved based on the parameters estimated in Step #1 and Step #2, even though no excitation current is injected in Step #3. It is validated that the battery parameter/state can be accurately identified using the sequential algorithm and the SIC is well addressed by the proposed MPC+.

In the comparison case, all parameters and states are identified based on the MPC– results shown in Fig. 4. The multi-scale EKF, which has been shown to be more effective than the dual EKF

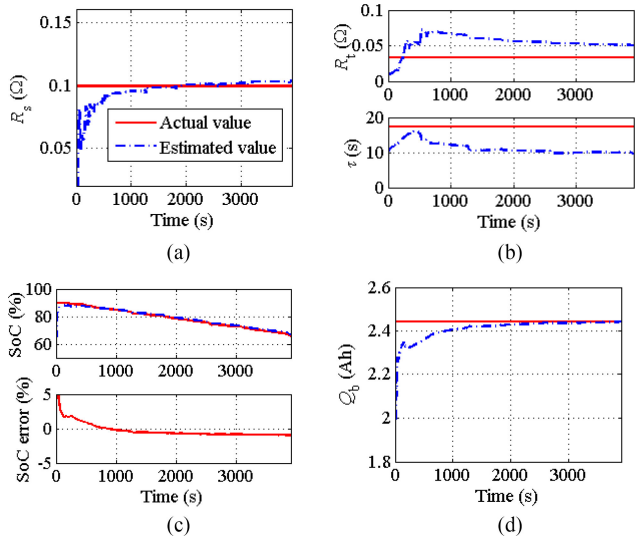

Fig. 10. Parameter identification result of MPC–. (a) R_s. (b) R_t and τ. (c) SoC. (d) Q_b.

[16], is adopted. The detailed information on the multi-scale EKF is provided in [16] and [37]. Since three consecutive driving cycles are involved in the identification process of MPC+, the identification of MPC– is also conducted using three consecutive current profiles. The identification results are shown in Fig. 10. As shown in Fig. 10(a) and (c), the identified R_s and Q_b converge to the actual values but with a longer time to converge when compared to MPC+. As shown in Fig. 10(b), the identified R_t and τ of MPC– cannot track the actual values and there are significant identification errors. As shown in Fig. 10(d), the static error of the identified battery SoC increases to 0.9%. As the estimation processes of different parameters and states influence each other and bring more uncertainty, the identification error of battery terminal voltage is enlarged by MPC–, as shown in Fig. 11.

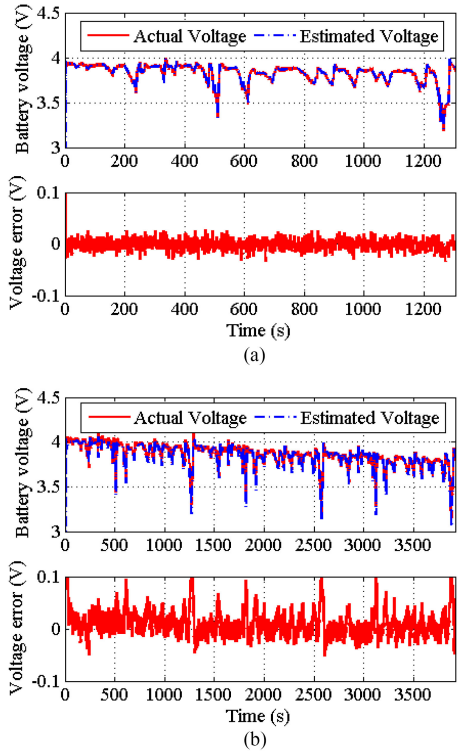

Fig. 11. Battery terminal voltage comparison. (a) MPC+. (b) MPC–.

C. Tradeoff Between Identification and Optimization

As illustrated above, the proposed MPC+ improves identification accuracy at the expense of an increase in energy loss. To further investigate the tradeoff between identification and optimization, the amplitudes of the injected current (i.e., I_{ex}) are fixed at various values and MPC+ is used for the optimization. The ohmic resistance is identified based on simulation results and the root mean square (rms) of the identification error is calculated. The value of I_{ex} ranges from 1 to 8 A, and the simulation results are shown in Fig. 12. This shows that the identification accuracy can be improved by increasing I_{ex}, which verifies the conclusion that the identification accuracy of battery parameters is related to the amplitude of the excitation current. However, energy loss also increases as I_{ex} increases. It is worth noticing that the identification accuracy can be significantly improved initially with an increasing I_{ex}; however, the effect of increasing I_{ex} on improving identification accuracy is not obvious for the I_{ex} beyond a transition area, where the "knee"

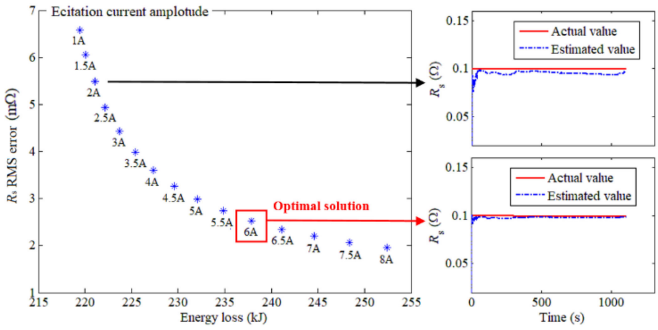

Fig. 12. Tradeoff between identification accuracy and system efficiency.

point (i.e., $I_{ex} = 6$A) can be found and selected as the optimal solution [38].

Parameter identification is also significantly influenced by measurement noise. To verify the robustness of the optimal amplitude of excitation current, the noise amplitude (in the voltage measurement) is varied in the simulation, and the identification of R_s is conducted under different levels of white noise. When the white noise amplitudes are 50% and 200% of the original value, the simulation results show similar trends when compared to the original result, as shown in Figs. 12 and 13. As a result, the optimal solution is robust to different noise levels.

Note that the rms error of R_s corresponding to MPC- is 12.5 mΩ. In comparison, when I_{ex} is 1 A the RMS error corresponding to MPC+ is 6.58 mΩ, indicating that the identification error can be reduced by 47.4% even when the injected current

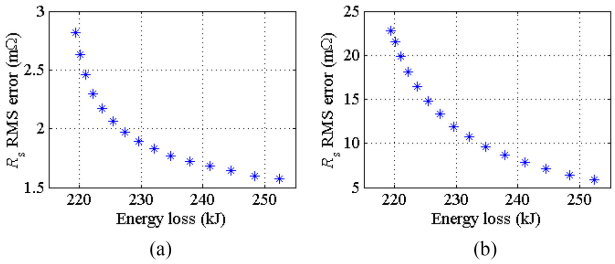

Fig. 13. Tradeoff under various white noise amplitudes. (a) 50% white noise. (b) 200% white noise.

is small. Therefore, the active current injection realized by the proposed MPC+ can significantly reduce the identification errors of battery parameters. Due to space limitations, tradeoffs associated with identification of the *RC* pair is not investigated here. We also note that the energy loss of MPC+ can be potentially reduced. As shown in Fig. 9, the identification of ohmic resistance and *RC* pair only takes 200 and 50 s, respectively. If desired, the identification periods of Step #1 and Step #2 can be turned OFF, and so MPC+ can be switched to MPC– to further reduce energy loss. In addition, the proposed MPC+ can be generalized to other overactuated systems with batteries (e.g., hybrid electric vehicles) to simultaneously achieve identification and loss minimization objectives [39].

This article emphasizes how to implement the sequential algorithm in overactuated systems (e.g., battery/supercapacitor HESS), and no experimental validation is presented here. However, we point out that the effectiveness and robustness of the sequential algorithm have been experimentally validated in other works. The detailed information can be found in [17] and [25].

V. Conclusion

A novel MPC was proposed in this article for handling simultaneous identification and optimization of HESS using active current injection. The overactuated feature of HESS was exploited to achieve accurate identification of battery state/parameter and satisfactory system efficiency simultaneously. The proposed MPC approach simultaneously considers the system efficiency, injected signal richness, and output power regulation. Simulation results showed that when compared to the baseline MPC without considering active current injection, the proposed MPC can effectively perform the SIC. Specifically, the proposed MPC significantly improves the identification accuracy of battery parameter/state (e.g., the rms errors of the estimated R_s and SoC can be both reduced by around 50%) at the expense of a slight increase in the energy consumption (i.e., around 0.4%). The tradeoff between identification accuracy and system efficiency was investigated and the optimal amplitude of the injected current, which achieves the best tradeoff and is robust to noise amplitude, was determined.

References

[1] P. Ioannou and J. Sun, *Robust Adaptive Control*, vol. 1. Chelmsford, MA, USA: Courier Corp., 2012.

[2] A. Dizqah, B. Lenzo, A. Sorniotti, P. Gruber, S. Fallah, and J. De Smet, "A fast and parametric torque distribution strategy for four-wheel-drive energy-efficient electric vehicles," *IEEE Trans. Ind. Electron.*, vol. 63, no. 7, pp. 4367–4376, Jul. 2016.

[3] D. Reed, J. Sun, and H. Hofmann, "Simultaneous identification and adaptive torque control of permanent magnet synchronous machines," *IEEE Trans. Control. Syst. Technol.*, vol. 25, no. 4, pp. 1372–1383, Jul. 2017.

[4] A. Hasanzadeh, D. Reed, and H. Hofmann, "Rotor resistance estimation for induction machines using carrier signal injection with minimized torque ripple," *IEEE Trans. Energy Convers.*, vol. 34, no. 2, pp. 942–951, Jun. 2019.

[5] Y. Chen and J. Wang, "Fast and global optimal energy-efficient control allocation with applications to over-actuated electric ground vehicles," *IEEE Trans. Control Syst. Technol.*, vol. 20, no. 5, pp. 1202–1211, Sep. 2012.

[6] A. Weiss, F. Leve, I. V. Kolmanovsky, and M. Jah, "Reaction wheel parameter identification and control through receding horizon-based null motion excitation," in *Proc. Symp. Estimation, Navig., Spacecraft Control*, 2015, pp. 477–494.

[7] K. Hu, P. Yi, and C. Liaw, "An EV SRM drive powered by battery/supercapacitor with G2V and V2H/V2G capabilities," *IEEE Trans. Ind. Electron.*, vol. 62, no. 8, pp. 4714–4727, Aug. 2015.

[8] W. Li, G. Joós, and J. Bélanger, "Real-time simulation of a wind turbine generator coupled with a battery supercapacitor energy storage system," *IEEE Trans. Ind. Electron.*, vol. 57, no. 4, pp. 1137–1145, Apr. 2010.

[9] J. Xiao, P. Wang, and L. Setyawan, "Hierarchical control of hybrid energy storage system in DC microgrids," *IEEE Trans. Ind. Electron.*, vol. 62, no. 8, pp. 4915–4924, Aug. 2015.

[10] Z. Song, J. Hou, H. Hofmann, X. Lin, and J. Sun, "Parameter identification and maximum power estimation of battery/supercapacitor hybrid energy storage system based on Cramer-Rao bound analysis," *IEEE Trans. Power Electron.*, vol. 34, no. 5, pp. 4831–4843, May 2019.

[11] M. Shahriari and M. Farrokhi, "Online state-of-health estimation of VRLA batteries using state of charge," *IEEE Trans. Ind. Electron.*, vol. 60, no. 1, pp. 191–202, Jan. 2013.

[12] Z. Song, H. Hofmann, J. Li, X. Han, X. Zhang, and M. Ouyang, "A comparison study of different semi-active hybrid energy storage system topologies for electric vehicles," *J. Power Sources*, vol. 274, pp. 400–411, Jan. 2015.

[13] M. Vasallo, J. Andújar, C. García, and J. Brey, "A methodology for sizing backup fuel-cell/battery hybrid power systems," *IEEE Trans. Ind. Electron.*, vol. 57, no. 6, pp. 1964–1975, Jun. 2010.

[14] Z. Song, H. Hofmann, J. Li, J. Hou, X. Han, and M. Ouyang, "Energy management strategies comparison for electric vehicles with hybrid energy storage system," *Appl. Energy*, vol. 134, pp. 321–331, Dec. 2014.

[15] N. Bertrand, J. Sabatier, O. Briat, and J. Vinassa, "Embedded fractional nonlinear supercapacitor model and its parametric estimation method," *IEEE Trans. Ind. Electron.*, vol. 57, no. 12, pp. 3991–4000, Dec. 2010.

[16] R. Xiong, F. Sun, Z. Chen, and H. He, "A data-driven multi-scale extended Kalman filtering based parameter and state estimation approach of lithium-ion olymer battery in electric vehicles," *Appl. Energy*, vol. 113, pp. 463–476, Jan. 2014.

[17] Z. Song, X. Wu, X. Li, J. Sun, H. Hofmann, and H. Jun, "Current profile optimization for combined state of charge and state of health estimation of lithium ion battery based on Cramer-Rao bound analysis," *IEEE Trans. Power Electron.*, vol. 34, no. 7, pp. 7067–7078, Jul. 2019.

[18] S. Choi, B. Akin, M. Rahimian, and H. Toliyat, "Performance-oriented electric motors diagnostics in modern energy conversion systems," *IEEE Trans. Ind. Electron.*, vol. 59, no. 2, pp. 1266–1277, Feb. 2012.

[19] P. Mishra, M. Garg, S. Mendoza, J. Liu, C. Rahn, and H. Fathy, "How does model reduction affect lithium-ion battery state of charge estimation errors? Theory and experiments," *J. Electrochem. Soc.*, vol. 164, no. 2, pp. A237–A251, 2017.

[20] X. Lin and A. Stefanopoulou, "Analytic bound on accuracy of battery state and parameter estimation," *J. Electrochem. Soc.*, vol. 162, no. 9, pp. A1879–A1891, 2015.

[21] A. Klintberg, T. Wik, and B. Fridholm, "Theoretical bounds on the accuracy of state and parameter estimation for batteries," in *Proc. Amer. Control Conf.*, 2017, pp. 4035–4041.

[22] M. Rothenberger, D. Docimo, M. Ghanaatpishe, and H. Fathy, "Genetic optimization and experimental validation of a test cycle that maximizes parameter identifiability for a Li-ion equivalent-circuit battery model," *J. Energy Storage*, vol. 4, pp. 156–166, Dec. 2015.

[23] M. Rothenberger, J. Anstrom, S. Brennan, and H. Fathy, "Maximizing parameter identifiability of an equivalent-circuit battery model using optimal periodic input shaping," in *Proc. ASME Dyn. Syst. Control Conf.*, 2014, paper DSCC2014-6272.

[24] X. Lin, "Theoretical analysis of battery SOC estimation errors under sensor bias and variance," *IEEE Trans. Ind. Electron.*, vol. 65, no. 9, pp. 7138–7148, Sep. 2018.
[25] Z. Song *et al.*, "The sequential algorithm for combined state of charge and state of health estimation of lithium ion battery based on active current injection," 2019, *arXiv:1901.06000*.
[26] J. Hou, J. Sun, and H. Hofmann, "Mitigating power fluctuations in electric ship propulsion with hybrid energy storage system: Design and analysis," *IEEE J. Oceanic Eng.*, vol. 43, no. 1, pp. 93–107, Jan. 2018.
[27] S. Feng, H. Sun, Y. Zhang, J. Zheng, H. X. Liu, and L. Li, "Tube-based discrete controller design for vehicle platoons subject to disturbances and saturation constraints," *IEEE Trans. Control Syst. Technol.*, to be published.
[28] J. Rathousk'y and V. Havlena, "MPC-based approximate dual controller by information matrix maximization," *Int. J. Adapt. Control Signal Process.*, vol. 27, no. 11, pp. 974–999, 2013.
[29] I. Kolmanovsky and D. P. Filev, "Optimal finite and receding horizon control for identification in automotive systems," in *Identification for Automotive Systems*. New York, NY, USA: Springer, 2012, pp. 327–348.
[30] G. Marafioti, R. Bitmead, and M. Hovd, "Persistently exciting model predictive control using fir models," in *Proc. Int. Conf. Cybern. Informat.*, 2010, pp. 1–10.
[31] X. Hu, S. Li, and H. Peng, "A comparative study of equivalent circuit models for Li-ion batteries," *J. Power Sources*, vol. 198, pp. 359–367, Jan. 2012.
[32] C. Weng, Y. Cui, J. Sun, and H. Peng, "On-board state of health monitoring of lithium-ion batteries using incremental capacity analysis with support vector regression," *J. Power Sources*, vol. 235, pp. 36–44, Aug. 2013.
[33] J. Wei, G. Dong, and Z. Chen, "Remaining useful life prediction and state of health diagnosis for lithium-ion batteries using particle filter and support vector regression," *IEEE Trans. Ind. Electron.*, vol. 65, no. 7, pp. 5634–5643, Jul. 2018.
[34] C. Zhang, K. Li, J. Deng, and S. Song, "Improved realtime state-of-charge estimation of $LiFePO_4$ battery based on a novel thermoelectric model," *IEEE Trans. Ind. Electron.*, vol. 64, no. 1, pp. 654–663, Jan. 2017.
[35] N. Samad, J. Siegel, and A. Stefanopoulou, "Parameterization and validation of a distributed coupled electro-thermal model for prismatic cells," in *Proc. ASME Dyn. Syst. Control Conf.*, 2014, paper DSCC2014-6321.
[36] Y. Gu *et al.*, "Design and flight testing evaluation of formation control laws," *IEEE Trans. Control Syst. Tech.*, vol. 14, no. 6, pp. 1105–1112, Nov. 2006.
[37] C. Hu, B. Youn, and J. Chung, "A multiscale framework with extended Kalman filter for lithium-ion battery SOC and capacity estimation," *Appl. Energy*, vol. 92, pp. 694–704, Apr. 2012.
[38] X. Zhang, Y. Tian, and Y. Jin, "A knee point-driven evolutionary algorithm for many-objective optimization," *IEEE Trans. Evol. Comput.*, vol. 19, no. 6, pp. 761–776, Dec. 2015.
[39] H. Zhu, Z. Song, J. Hou, H. Hofmann, and J. Sun, "Simultaneous identification and control using active signal injection for series hybrid electric vehicles based on dynamic programming," 2019, *arXiv:1909.08062*.

Ziyou Song (M'18) received the B.E. (Hons.) and Ph.D. degrees (with highest honor and thesis award) in automotive engineering from Tsinghua University, Beijing, China, in 2011 and 2016, respectively.

He worked as a Research Scientist with Tsinghua University from 2016 to 2017 and is currently a Postdoctoral Research Fellow with the Department of Naval Architecture & Marine Engineering, and the Department of Electrical Engineering and Computer Science, University of Michigan, Ann Arbor, MI, USA. He has authored or coauthored more than 50 peer-reviewed publications including more than 40 journal articles. His research interests include the areas of modeling, estimation, optimization, and control of energy storage for electrified vehicles and renewable systems.

Dr. Song was the recipient of several paper awards, including the Applied Energy 2015 to 2016 Highly Cited Paper Award, the Applied Energy Award for Most Cited Energy Article from China, the NSK Outstanding Paper Award of Mechanical Engineering, and the 2013 IEEE VPPC Best Student Paper Award.

Hyeongjun Park (M'16) received the B.S. and M.S. degrees from Seoul National University, Seoul, South Korea, in 2003 and 2008, respectively, and the Ph.D. degree from the University of Michigan, Ann Arbor, MI, USA, in 2014, all in aerospace engineering.

From 2015 to 2017, he was a Postdoctoral Research Associate with the U.S. National Research Council, Naval Postgraduate School, Monterey, CA, USA. He is currently an Assistant Professor with the Department of Mechanical and Aerospace Engineering, New Mexico State University, Las Cruces, NM, USA. His current research interests include real-time optimal control of constrained systems, guidance and control of spacecraft proximity operations, and autonomous aerial manipulation for interaction with the environment.

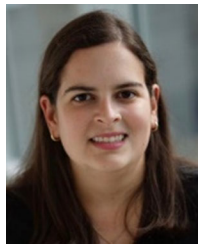

Fanny Pinto Delgado (S'18) received the Bachelor of Science degree in electrical engineering from Universidad Simon Bolivar, Caracas, Venezuela, in 2014, and the Master of Science degree in electrical engineering systems from The University of Michigan, Ann Arbor, MI, USA, in 2017. She is currently working toward the Ph.D. degree with the Electrical and Computer Engineering Department, The University of Michigan. She works under the guidance of Prof. Heath Hofmann and Prof. Jing Sun.

Her current research interests include condition monitoring and control of electric machines.

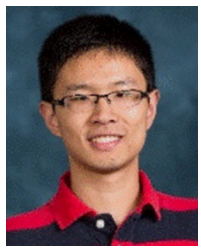

Hao Wang received the B.E. degree in vehicle engineering from the Hefei University of Technology, Hefei, China, in 2012, and the M.S.E. degree in mechanical engineering in 2014 from the University of Michigan, Ann Arbor, MI, USA, where he is currently working toward the Ph.D. degree in naval architecture and marine engineering.

His current research interests include set-membership identification and its applications, energy management of integrated power and thermal management systems, and applications to electrified vehicles.

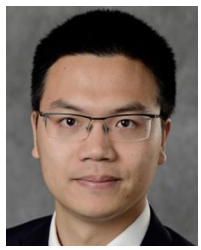

Zhaojian Li (S'15–M'16) received the bachelor's degree in civil aviation from the Department of Civil Aviation, Nanjing University of Aeronautics and Astronautics, Nanjing, China, and the M.S. and Ph.D. degrees in aerospace engineering (flight dynamics and control) from the University of Michigan, Ann Arbor, MI, USA, in 2013 and 2015, respectively.

From 2016 to 2017, he has worked as an Algorithm Engineer with General Motors. He is currently an Assistant Professor with the Department of Mechanical Engineering, Michigan State University, East Lansing, MI, USA. His research interests include learning-based control, nonlinear and complex systems, and robotics and automated vehicles. He received the National Scholarship from China.

Heath F. Hofmann (S'90–M'92–SM'16) received the Ph.D. degree in electrical engineering and computer science from the University of California at Berkeley, Berkeley, CA, USA, in 1998.

He is currently a Professor with the Department of Electrical Engineering and Computer Science, University of Michigan, Ann Arbor, MI, USA. He has authored approximately four dozen papers in refereed journals. He currently holds 14 patents. His research interests include power electronics, specializing in the design, simulation, and control of electromechanical systems, adaptive control techniques, energy harvesting, flywheel energy storage systems, electric and hybrid electric vehicles, and finite-element analysis.

Jing Sun (M'89–SM'00–F'04) received the B.S. and M.S. degrees from the University of Science and Technology of China, Hefei, China, in 1982 and 1984 respectively, and the Ph.D. degree from the University of Southern California, Los Angeles, CA, USA, in 1989, all in electrical engineering.

From 1989 to 1993, she was an Assistant Professor with the Electrical and Computer Engineering Department, Wayne State University. She joined Ford Research Laboratory in 1993, where she worked in the Powertrain Control Systems Department. After spending almost ten years in industry, she came back to academia and joined the faculty of the College of Engineering, University of Michigan, Ann Arbor, MI, USA, in 2003, where she is currently a Michael G. Parsons Professor and the Chair with the Department of Naval Architecture and Marine Engineering, with courtesy appointments as a Professor with the Department of Electrical Engineering and Computer Science and the Department of Mechanical Engineering. Her research interests include system and control theory and its applications to marine and automotive propulsion systems. She holds 39 U.S. patents and has coauthored a textbook on *Robust Adaptive Control*.

She was the recipient of the 2003 IEEE Control System Technology Award.

Jun Hou (S'15–M'18) received the M.S. degree in electrical engineering from Northeastern University, Shenyang, China, in 2011, and the Ph.D. degree in electrical and computer engineering from the University of Michigan, Ann Arbor, MI, USA, in 2017.

His current research interests include integration, modeling, control, and optimization of hybrid energy storage, power electronic converters, and electric propulsion systems.